Article

Combined Experimental and Theoretical Insights: Spectroscopic and Molecular Investigation of Polyphenols from *Fagonia indica* via DFT, UV−vis, and FT-IR Approaches

Rabia Riaz, Shagufta Parveen, Maryam Rashid, and Nusrat Shafiq*

Read Online

ACCESS | Metrics & More | Article Recommendations | Supporting Information

ABSTRACT: This review deals with computational study of polyphenolic compounds of medicinal importance and interest for drug development. Herein, four polyphenolic compounds comprising catechol (**1**), caffeic acid (**II**), gallic acid (**III**), and pyrogallol (**IV**) have been isolated from a medicinal specie, *Fagonia indica,* by applying silica gel column chromatography. These compounds were identified by using gas chromatography−mass spectrometry (GC−MS) analysis and confirmed by geometric computational analysis. According to computational results, caffeic acid has shown the highest biological activation due to higher chemical softness, electronegativity (χ (eV) = −648.644), and electrostatic potential value (-8.424×10^{-2} to $+8.424 \times 10^{-2}$), while smaller values of chemical potential (−0.269), E_{LUMO} (−0.080), and energy gap ($\Delta E = 0.149$). The Mulliken atomic charges were calculated by using DFT/B3LYP with basis set 6-311G for the determination of active sites. The oxygen atom of catechol showed highest nucleophilic characteristic with a more negative charge (08 = −0.695), and pyrogallol indicated a strong electrophilic center at C14 = 0.415 with a higher positive charge. Moreover, UV−visible absorption spectra and a detailed study of vibrational frequencies for all phenolic compounds by employing the DFT approach with 3-21G, 6-31G, and 6-311G basis sets at the ground-state level showed the great agreement with experimental results. ANOVA has been applied to validate the theoretical data. Results suggest that compounds **I**−**IV** are suitable in diverse fields.

1. INTRODUCTION

Medicinal plants are vast resources of essential natural constituents with huge potential to be used as novel therapeutic drugs. Depiction of blue, red, and purple color in natural products, i.e., vegetables and fruits, directly relate with the presence of polyphenols. The natural polyphenolic compounds extracted from dietary plants and medicinal herbs possess a number of beneficial health effects and also play an important role for cancer inhibition as well as treatment. Pharmacological studies of *Fagonia indica* showed that this specie is very essential due to its use in hematological, hepatic, and neurological disorders;[1] these applications are directly linked with important chemical constituents present in it like sterols, flavonoids, polyphenolic compounds, saponins, and terpenoids, which are predominantly reported in this plant.[2]

The natural polyphenolic compounds are substantial materials because of their implications in numerous sectors such as conservative agents, natural additives, natural coloring agents, and natural antioxidants in the food-processing industry, and these are also very good for human health. Many plant species containing phenolic constituents of interest may be used as food supplements or can be incorporated into pharmaceutical formulations and cosmetics as well.[3] Polyphenols are the essential dietary antioxidants and are widely distributed in plants.[4]

The natural phenolic compounds include flavonoids, phenolic acids, tannins, curcuminoids, stilbenes, coumarins, quinones, lignans, etc. Numerous chemopreventive properties and bioactivities of phenolic compounds are responsible for their activation as anticarcinogenic, antioxidant[5] and anti-inflammatory compounds. Natural polyphenols also contribute to inducing apoptosis through cell cycle arrest, regulating carcinogen metabolism and ontogenesis expression by inhibiting cell adhesion and DNA binding, cell differentiation, or proliferation and by blocking signaling pathways.[6] These are widely investigated for clinical purposes due to their significance in the diagnosis of salivary glands and pancreas. Furthermore, polyphenols are main precursors of novel drug design for the treatment of various diseases such as hyperlipidemia, cancer, liver diseases, diabetes etc.

In accordance with the literature review, these natural compounds possess numerous health beneficial roles such as against oxidative stress, cardiovascular risk, hypertension, endothelial dysfunction, atherogenesis, diabetes, lipid disorders, and carotid artery intima-media thickness.[7]

Polyphenols contain one or more hydroxyl groups and at least one aromatic ring in their structure. Considering their chemical structure, the polyphenols are divided into four main classes regarding their chemical groups and chemical formulas.[8] The major classes of polyphenols are compounds
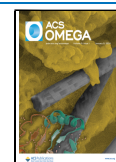
with one C6 aromatic ring of hydroxybenzoic acids including phenolic acids such as tannins, gallic acid, and hydroxytyrosol[9] and others with a C6−C3 structure of hydroxycinnamic acids, i.e., coumaric acid and caffeic acid, those with the structure of stilbenes (C6−C2−C6) such as resveratrol including the catecholic group, those with the flavonoid structure (C6−C3−C6), and another class with the structure of lignins (C6−C4−C6) such as secoisolariciresinol. A weak diprotic acid (1,2-dihydroxybenzene) is catechol, which presents a wide range of environmental and biological applications. In natural organic compounds, among several oxygen-containing functional groups, catechol is a metabolic intermediate for microbial degradation. It is a highly reactive group and readily undergoes oxidative polymerization reactions to form complexes with other species. It exhibits strong antioxidant characteristics.[10]

Our literature survey reveals that there are no published studies on reactivity comparison of the above-mentioned natural polyphenols through quantum chemical description, electronic charge distribution, and geometric and spectroscopic account details.[11] The main aim of the present research is to obtain polyphenolic compounds from a remedial plant, *F. indica*, through computation analysis of various parameters of these isolated species regarding their importance in biological systems.[12] Moreover, the correlation of the biological activation of compounds with their molecular constraints has also been provided by DFT calculations. Another objective of the current research is to elaborate more accurate and precise chemical concepts about molecular structure by optimizing their parameters through quick and economic computational methods as compared to costly and laborious experimental systems.[13−15]

For correct identification of novel drug candidates isolated from a natural source, a potentially powerful analytical tool, "GC−MS", along with computational approaches has been applied for final structure verification of these candidates.[16] Density functional theory (DFT) calculations revealed the biochemical reactivity order for compounds and specifies active sites within the molecules,[17] which is very essential for biological systems. Moreover, computer simulations of IR vibrations and UV−vis spectroscopy by DFT make this study routinely useful in several areas of experimental research and a crucial tool for the analysis of experimental results. In particular, it has turned out to be the line of choice for describing the structural properties of polyphenolic compounds. The motive behind the present study lies in the fact that it provides precise results for medium-sized phenolic compounds at a low computational cost.

For these purposes, the natural polyphenols (**I**, **II**, **III**, and **IV**) were obtained from a selected medicinal herb by using silica gel column chromatography followed by thin-layer chromatography (TLC) and characterized by GC−MS.

Computational studies have been accomplished by employing DFT with the B3LYP/3-21G, B3LYP/6-31G, and B3LYP/6-311G basis sets at the ground-state level. The quantum chemical descriptors that were predominantly used by computational researchers are computed for the investigation of molecular structure. The effect of electronic population on molecular active site has been computed by employing the Mulliken charge approach. UV−vis spectra have also been recorded for all compounds by TD-DFT.[18] Spectroscopic features have also been investigated by optimizing their FT-IR vibrational parameters with variable basis sets. The presentation of graphics and structures optimized by the Gaussian 09

program favored by the Gauss View 6.0 interface was applied successfully.[19,20] The geometrical optimization of molecules by using the hybrid-type B3LYP functional with a standard basis set in the alignment of DFT provides various molecular descriptors which correspond toward SAR.[21]

2. MATERIALS AND METHODS

2.1. Experimental Section. The polyphenols (**I−IV**) were isolated from a medicinal plant, *F. indica,* by applying chromatographic techniques. First, normal silica gel column chromatography was applied to obtain the semipure fraction from a crude plant extract.[22] In order to achieve this, different types of mobile phases were applied depending on polarity order. The purification of the semipure fraction was accomplished by using repeated silica gel column chromatography. Column chromatography was performed by means of LR-60 silica gel (60−100 mesh) as a stationary phase packed in glass columns eluted by gradients of organic solvents. Aluminum sheets percolated with silica gel 60 F254 (20 × 20 cm, 0.2 mm thick; E-Merck; Darmstadt, Germany) were used to monitor the chromatographic separations. The progress of chromatographic separation was monitored by applying TLC. A UV lamp at 254 and 366 nm has been used to observe the fluorescence of TLC profiles. Chromatogram was further monitored with locating agent (ceric sulfate) sprayed on chromatograms followed by heating to trace the UV-inactive metabolites. The semipure compounds obtained from the specie were identified by using spectroscopic technique GC−MS.[23]

2.2. Computational Profile. To calculate the quantum chemical parameters of phenolic compounds, GaussView 6.0, ChemDraw Version (19.1), Chem 3D 19.1, and Gaussian 09[24] Revision-D.01-SMP[25,26,26,27] programs were used frequently.[28] For the calculations of geometric parameters, DFT was used at the Becke3−Lee−Yang−Parr (B3LYP) level with an extended basis set, 6-311G.[29] The vibrational analysis of polyphenolic compounds, i.e., (**I**) catechol, (**II**) caffeic acid, (**III**) gallic acid, and (**IV**) pyrogallol, has been carried by employing DFT with 6-311G/B3LYP and the IEFPCM solvent effect model with three different basis solvents, i.e., acetonitrile, methanol, and chloroform. UV−vis absorption spectra of polyphenols (**I** to **IV**) were computed by TD-DFT with 3-21G, 6-31G, and 6-311G basis sets at the ground-state level.[30] For the IR vibrational analysis of compounds, DFT/B3LYP with three different basis sets, i.e., 6-31G, 6-311G, and 3-21G, was employed.[31] Various quantum chemical parameters including the energy of the lowest unoccupied molecular orbital (E_{LUMO}), energy of the highly occupied molecular orbital (E_{HOMO}), and energy gap between LUMO and HOMO (E_{GAP}) have been investigated. Moreover, absolute softness (σ), absolute hardness (η), absolute electronegativity (χ), electrophilicity index (ω), chemical potential (CP), nucleophilicity index (N), additional electronic charges (ΔN_{max}), electronic energy (E), dipole moment (μ), and global softness (S) have been calculated. The DFT approach has been applied with the B3LYP/6-311G functional and following formulas used to calculate these descriptors.[32]

$$I = -E_{HOMO} \tag{1}$$

$$A = -E_{LUMO} \tag{2}$$

$$E_{GAP} = E_{LUMO} - E_{HOMO} \tag{3}$$

$$\eta = I - A/2 = E_{\text{LUMO}} - E_{\text{HOMO}}/2 \qquad (4)$$

$$\sigma = 1/n \qquad (5)$$

$$\chi = 1 + A/2 \qquad (6)$$

$$\text{CP} = -\chi \qquad (7)$$

$$\omega = \text{CP}^2/2\eta \qquad (8)$$

$$N = 1/\omega \qquad (9)$$

$$\Delta N_{\text{max}} = -\text{CP}/\eta \qquad (10)$$

$$S = 1/2\eta \qquad (11)$$

All results for the calculated data are discussed in detail in their respective sections.

3. RESULTS AND DISCUSSION

3.1. Identification of Isolated Compounds. The semipure alcoholic fraction of *F. indica* was subjected to GC−MS analysis. The mass spectrometer detector (MSD) in NIST analyzed the spectral data of unknown compounds through library search in the form of compound hit list based on their match factor, reverse match factor, and probability (%) score in comparison to reference standards of library. The results have displayed number of peaks, but the tentative identification of compounds has been confirmed for the species with distinct retention time, MF and RMF > 900, possessing good probability value for the first hit in the compound hit list, while the peaks with MF and RMF below 600 were considered uncertain. On the other hand, probability score variations among adjacent hits in the hit list gave the value of relative probability, which decides the perfect hit through perfect match.[33] According to the interpretation of NIST search library factors, peaks 1−4 (Table 1) have confined for polyphenolic species enlisted in table with perfect match to standards of library.

Table 1. NIST Data of GCMS Analysis of Isolated Compounds

sample	peak #	RT (min)	match	R. match	prob (%)	compound name
methanol extract	1	4.0843	930	946	97.9	caffeic acid
	2	6.075	890	929	43.8	catechol
	3	6.832	723	732	9.6	gallic acid
	4	9.241	772	830	62.9	pyrogallol

3.2. FT-IR Vibrational Analysis of Polyphenolic Compounds. GaussView 6.0 has been used for IR-vibrational calculations, and their visualization has been accompanied by animation options. Compound (**I**) with 14 number of atoms possess 36 vibrational modes, while compound (**II**) containing 21 atoms will indicate 57 fundamental vibrational modes. Compound (**III**) containing 18 atoms has shown 48 vibrations, and compound (**IV**) with 15 atoms has shown 39 IR-vibrational frequencies according to the 3N-6 rule.[34] The IR spectra of these polyphenols taken by DFT with different solvents have been compared (Figure 1), and the calculated frequencies were compared with their respective experimental values (from the literature).

The DFT calculations with implicit solvent (IEFPCM = integral equation formalism polarizable continuum model)

indicate that the dielectric constant of solvents has small influence on vibrational band position, while the alcoholic solvents like methanol caused the upshifting of vibrational frequencies due to H-bonding.[35]

All of the vibrational modes have numbered from largest to smallest wavenumber values.[36] Assignments for all vibrational modes (from the literature) have also been presented in Table S1 (Supporting Information), respectively.

3.2.1. O−H Vibrations. O−H vibrations are most sensitive vibrations and may play a fundamental role in structural description, as if intramolecular H-bonding will be present, it can reduce the O−H stretching bands as compared to OH-free molecules.[37] According to the results of Gaussian calculations of polyphenols, applied through DFT/B3LYP with the 6-311G basis set for all the three solvents, the νOH stretching vibrations lie in the region of IR spectra with higher wavenumber values; this occurs for most of the organic compounds.[31] These values range approximately from 3700 to 3200 cm^{-1} for all compounds. While δOH in plan bending vibrational modes gave bands at a range of 1300−1200 cm^{-1}, βOH deformations appear at 1400−1100 cm^{-1}, but γOH and τOH vibrational modes assign with smaller wavenumber in IR vibrational spectra, i.e., 700−500 and 400−170 cm^{-1}, respectively.

3.2.2. C−H Vibrations. The νCH stretches of polyphenols deceit in the range of 3200−3100 cm^{-1}, while in plan bending δCH, βCH appears at 1200−1100 cm^{-1} and out of plan γCH bending vibrations lie in the range of 900−800 cm^{-1} in the infrared spectrum of compounds under investigation. The most striking results were obtained in the range of 1200−1100 cm^{-1}, indicating that the calculations with solvent implicit in this region of the IR spectrum are less sensitive to the type of solvent used and are free from the dielectric constant around the molecule.

3.2.3. Ring Stretching and Deformation Modes. νCC stretching vibrations are very prominent and have the characteristics of an aromatic ring, and these vibrations are commonly expected to occur at 1600−1200 cm^{-1}.[38] According to the results of compounds under investigation, νCC stretching vibrations mixed with some CO and βOH characteristics gave polarized bands with wavenumber values ranging from 1600 to 1500 cm^{-1} in the IR spectrum of compounds, while the ring deformations with δCCC and γCCC mostly fall at lower frequency regions from 700 to 180 cm^{-1}.

3.2.4. C−O Vibrations. For the IR spectrum of alcoholic and phenolic compounds, mostly νCO stretching occurs at 1200−1000 cm^{-1} and appears as a strongest band,[39] but νCO stretches mixed with βOH and βCH characteristics gave bands at 1400−1300 cm^{-1}. Almost all IR-computed values for polyphenols (**I−IV**) by DFT/B3LYP at three different basis sets closely correlate among each other and with their corresponding experimental FT-IR values, but notable differences were observed in calculated and experimental OH stretching vibrations. These deviations can be explained by the fact of hydrogen bond formation[36] that are neglected in simulated spectra but particularly important in real solid state.[40] This hydrogen bonding specifically effects the shifting of OH stretching vibrations toward lower frequency regions, resulting in broadening and mixing of different vibrational modes.

Computed values showed close coherence with corresponding experimental values, while the differences are due to phase
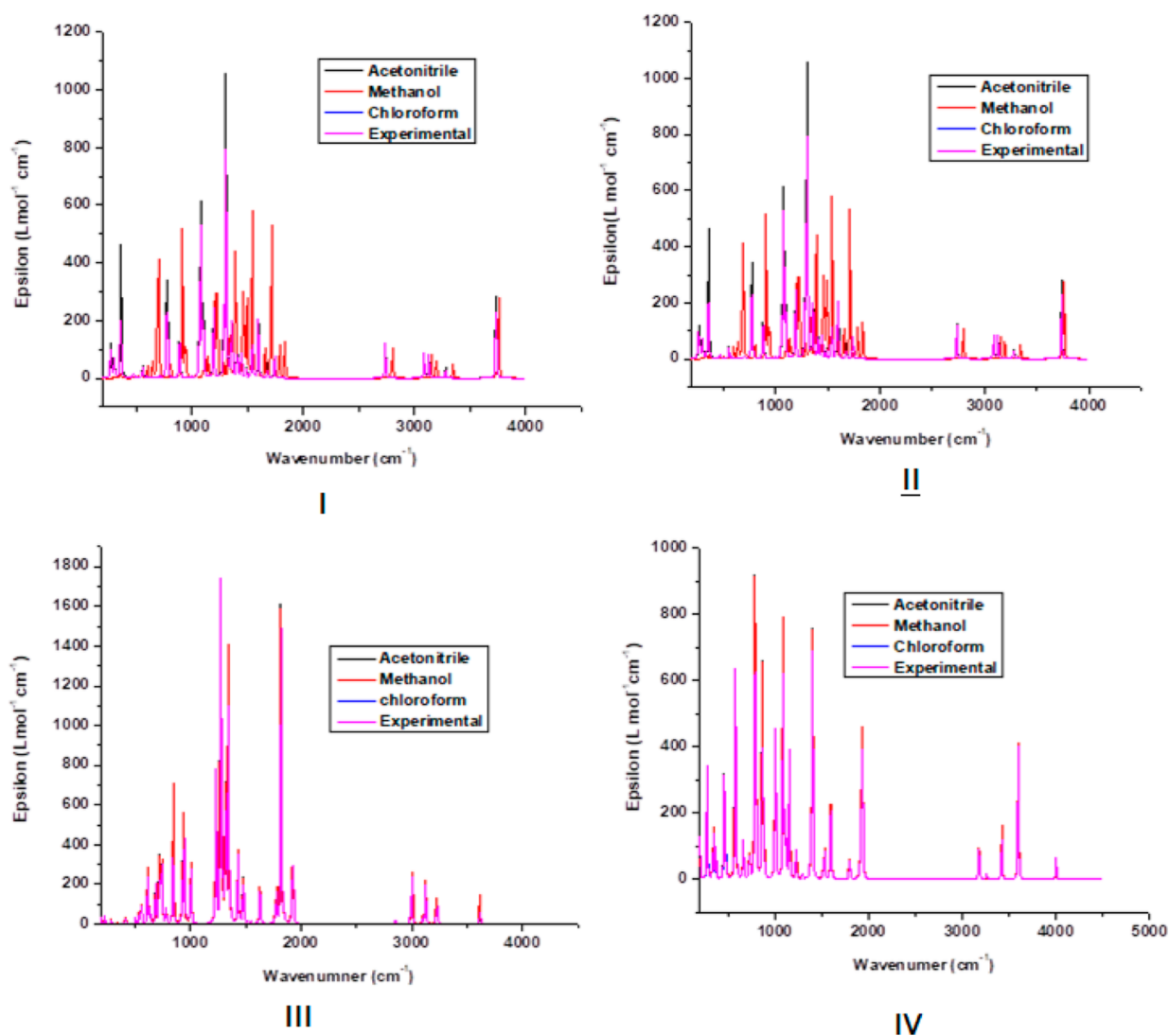
Figure 1. Experimental and simulated IR spectra of polyphenols (**I−IV**) at three different solvents.

changes among the computed (ground-state) and experimental (solid-state) vibrational frequencies. On the other hand, the values computed by DFT with different solvents possess subsequent systematic errors, which can be corrected by applying scaling factors.[41]

3.3. Frontiers Molecular Orbitals and Molecular Electrostatic Potential Analysis. For best results, under-study molecular structures were optimized by the DFT/B3LYP/6-311G basis set, and their optimized structures are given in Figure 2.
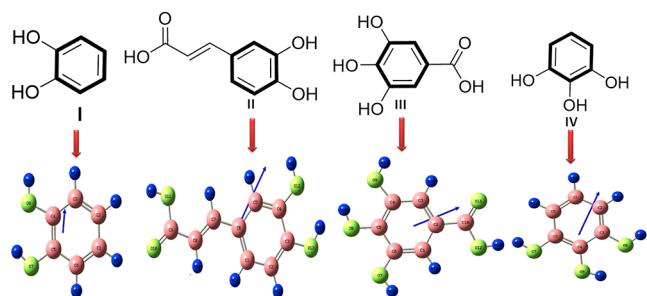

Figure 2. Optimized and molecular structures of compounds (**I−IV**).

Chemical parameters calculated to optimize polyphenols were found in agreement with those in Table 2.

According to the prescribed recommendations about calculated chemical parameters, the highest values of E_{HOMO} indicate the electron donation capability of the particular compound toward the appropriate acceptor which in turn leads to the reactivity or biological activation of that specie toward electron-accepting molecular entities.[42] So, according to the values calculated in Table 1 with consistently higher values of E_{HOMO}, the compound reactivity will follow a trend

Pyrogallol (**IV**) > catechol(**I**)

> caffeic acid (**II**)

> gallic acid (**III**)
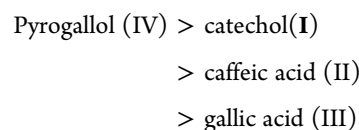
While the lower values of E_{LUMO} indicate that compounds possess good electron-accepting capability and serve as a reactive species for electron-donating compounds, reactivity trails the trend in the following order

Table 2. Calculation of Quantum Chemical Parameters for Polyphenols

quantum chemical parameters	catechol (I)	caffeic acid (II)	gallic acid (III)	pyrogallol (IV)
E_{LUMO} (eV)	−0.007	−0.080	−0.064	0.002
E_{HOMO} (eV)	−0.222	−0.229	−0.233	−0.216
Energy Gap $\Delta E = E_{LUMO} - E_{HOMO}$ (eV)	0.215	0.149	0.169	0.217
$-E_{LUMO}$ A (eV)	0.007	0.080	0.064	−0.002
$-E_{HOMO}$ I (eV)	0.222	0.229	0.233	0.216
dipole moment μ (Debye)	2.954	4.541	1.121	3.617
chemical hardness η (eV) $I - A/2 = \Delta E/2$	0.107	0.075	0.085	0.108
absolute softness $\sigma = 1/\eta$	9.305	13.421	11.789	9.179
global softness $S = 1/2(\eta)$	4.653	6.710	5.894	4.589
electronegativity χ (eV) $I + A/2$	0.118	0.269	0.180	0.215
electrophilicity index $(\omega) = (CP)^2/2\eta$	0.065	0.486	0.192	0.213
electronic energy E (Hartree)	−382.806	−648.644	−646.452	−457.887
chemical potential $CP = -\chi$	−0.118	−0.269	−0.180	−0.215
nucleophilicity index $N = 1/(\omega)$	15.340	2.059	5.213	4.689
additional electronic charges ΔN_{max} (eV) $= -CP/\eta$	1.101	3.610	2.1268	1.979

Caffeic acid (**II**)> Gallic acid (**III**)> Catechol (**I**)> Pyrogallol (**IV**)
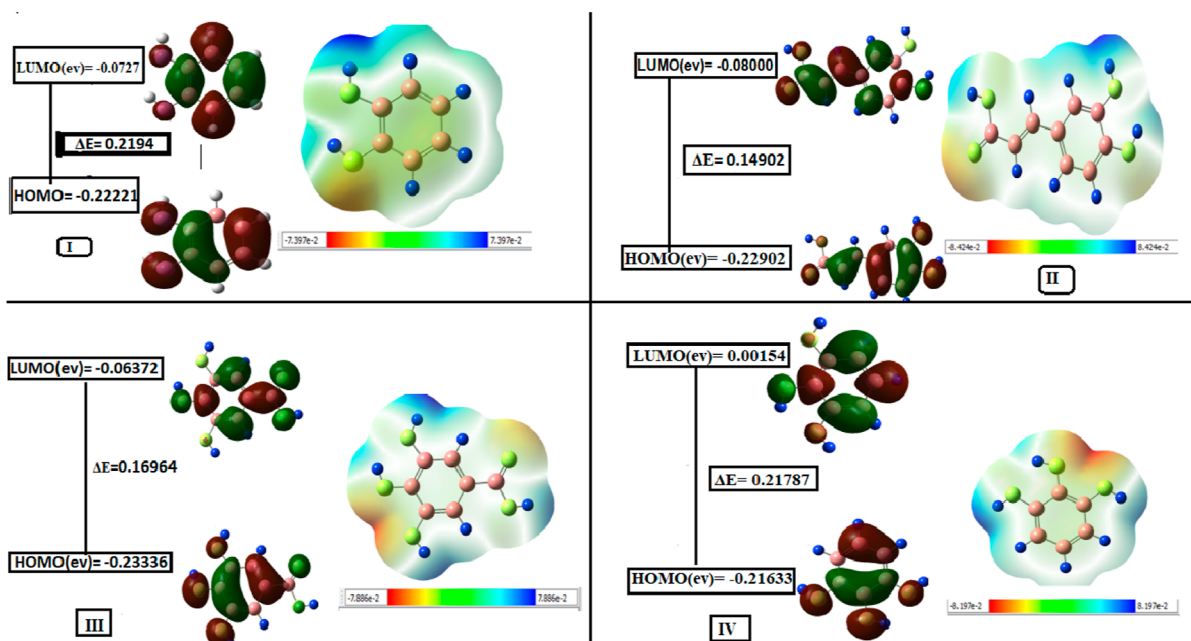

Figure 3. Contour diagram for FMOs and molecular electrostatic potential diagram.

Caffeic acid (II) > gallic acid (III)

> catechol (I)

> pyrogallol (IV)

Another quantum chemical parameter is the energy gap between two states HOMO and LUMO.[21,43,44] The gap between frontier molecular orbital (HOMO and LUMO) not only reflects the molecular stability but also related to molecular interaction with other species.[45] The lesser energy gaps make the molecules softer and corresponds toward reactiveness and less kinetic stability, so the biological activity of the compounds increases with smaller energy gaps. The reactivity trend for the calculated values of compounds should be as

Caffeic acid (II) > gallic acid (III) > catechol (I)

> pyrogallol (IV)

One more property associated with FMOs (Figure 3) is chemical hardness and softness; these are reciprocal of each other; zero chemical hardness means maximum chemical softness.[45] This parameter could be explained according to the HSAB concept, according to which "Hard molecules have larger energy gaps than soft molecules". As the biological system consists of cells and enzymes that are soft, therefore, they tend to coordinate more easily with soft molecules than the harder one. So, in the context of global softness and hardness, increasing order of biological activation for the corresponding compound will be as follows.[43]

Caffeic acid (**II**) > gallic acid (**III**) > catechol (**I**)

> pyrogallol (**IV**)

The global reactivity parameters are also associated with molecules' biological activity and are explained according to Koopman's theorem which is a useful and fast approach.[46]

Greater values of electronegativity and lower values of chemical potential facilitate biological activation of compounds due to the large measuring values of electronic transfer, as the compounds with delocalized electronic clouds can easily coordinate with biological systems. So, the activity ranking should be

Caffeic acid (**II**) > pyrogallol (**IV**) > gallic acid (**III**)

> catechol (**I**)

Conclusively, we could say that

High electronegativity ∝ biological activation

Low chemical potential ∝ biological activation

The molecules with higher values of electrophilicity are more reactive than others because of their electron-transfer potential. So, the biological activation of a molecule increases with higher values of nucleophilicity (N) and decreases with the lower values of electrophilicity (ω). The interaction of these molecules with the alpha amylase protein directs the best binding affinities for virtual screening of the antidiabetic potential of natural compounds in novel drug discovery processes. Considering this parameter, compound (**I**) shows lowest electrophilicity and highest nucleophilicity; thus, natural polyphenols (**I–IV**) follow a reactivity order

Catechol (**I**) > gallic acid(**III**)

> pyrogallol (**IV**)

> caffeic acid (**II**)

The compounds with higher values of dipole moment (μ) refer to increasing bond distances and better charge distribution, so they are localized molecules or more electrophilic systems, which refer to improved conductivity through oxidation processes, while the molecules having a smaller dipole moment may accept less electronic charge than the molecules of the high dipole moment.

Caffeic acid (**II**) > pyrogallol (**IV**) > catechol (**I**) > gallic

acid (**III**)

Large negative value of electronic energy (E) indicates the stability or low reactivity of compounds.[47]

The MEP description (Figure 3) facilitates in understanding the intra- and intermolecular connections like H-bonding, electrophilic, and nucleophilic interactions with incoming species and also helps in recognizing the type of biological interactions like drug protein interactions or molecular docking. Furthermore, it exhibited the behavior and response of molecules toward the binding sites in the biological system. The MEP of polyphenolic compounds composed by DFT/B3LYP with 6-311G is shown in Figure 3 based on the SCF energy. As it is the visual display for the assessment of molecular polarity, the positive (blue) part of MEP indicates the attacking site of the nucleophile, while the negative (yellow

and red) part indicates the attacking sites of the electrophilic molecule. More blue color is depicted by hydrogen atoms bonded with highly electronegative atoms, while red- and orange-colored region is depicted by oxygen atoms of carbonyl and hydroxyl groups, while neutral atoms of the benzene ring are indicated by pale green areas. According to the MEP surface, the electrostatic potential values related to color code maps increase in the order[48]

Red < orange < yellow < green < blue

Localization of orange or red color over oxygen atoms and localization of blue color over hydrogen atoms of benzene rings and hydroxyl substituents is responsible for the best radical scavenging activity.[15,44,49]

When electrostatic potential values of all the four compounds (given in Table 3) are compared to the reactivity order of compounds follows a trend

Caffeic acid (**II**) > pyrogallol (**IV**) > gallic acid (**III**)

> catechol

Table 3. Electrostatic Potential of Targeted Molecules (I–IV)

compounds	electrostatic potential values
(**I**)	-7.397×10^{-2} to $+7.397 \times 10^{-2}$
(**II**)	-8.424×10^{-2} to $+8.424 \times 10^{-2}$
(**III**)	-7.886×10^{-2} to $+7.886 \times 10^{-2}$
(**IV**)	-8.197×10^{-2} to $+8.197 \times 10^{-2}$

A good approximation is depicted by optimized geometric characters as it is a base for the calculation of other thermodynamic parameters. The optimized geometric parameters are calculated by applying DFT/B3LYP 6-311G for all compounds (**I–IV**). There are mainly four types of bonds in the mentioned polyphenolic compounds including C–C, C–O, and C–O; these bond lengths and bond angles (Table S2: Supporting Information) are calculated by DFT and compared with their experimentally determined or standard values given in the literature. Almost all computed bond lengths and bond angles indicate good agreement with their experimental values,[36] thereby confirming the structure of identified molecules. While some of the bond lengths and bond angles showed acceptable differences from experimental values, these differences are due to attachment of the hydroxyl group to the phenyl ring, which may distort molecular geometry. On the other hand, the presence of OH groups at consecutive positions (catechol group) on the ring may result in dimer formation and changing the values of bond lengths and bond angles, i.e., O–H, C–H, C–C, CCC, COH, and CCO from standard values.[36] Discrepancies among computational and experimentally determined values are due to variations in OH conformations. Moreover, almost all of the calculated values of bond angles and bond lengths are slightly higher than experimental values; this is due to phase differences, i.e., experimental values are taken in the solid state, and in this phase, intermolecular interactions connect the molecules together, while calculated data is obtained usually at the gas-phase or ground-state level.[48] Some calculated values are not correlated with their experimental values due to nonavailability of experimental data in the literature.
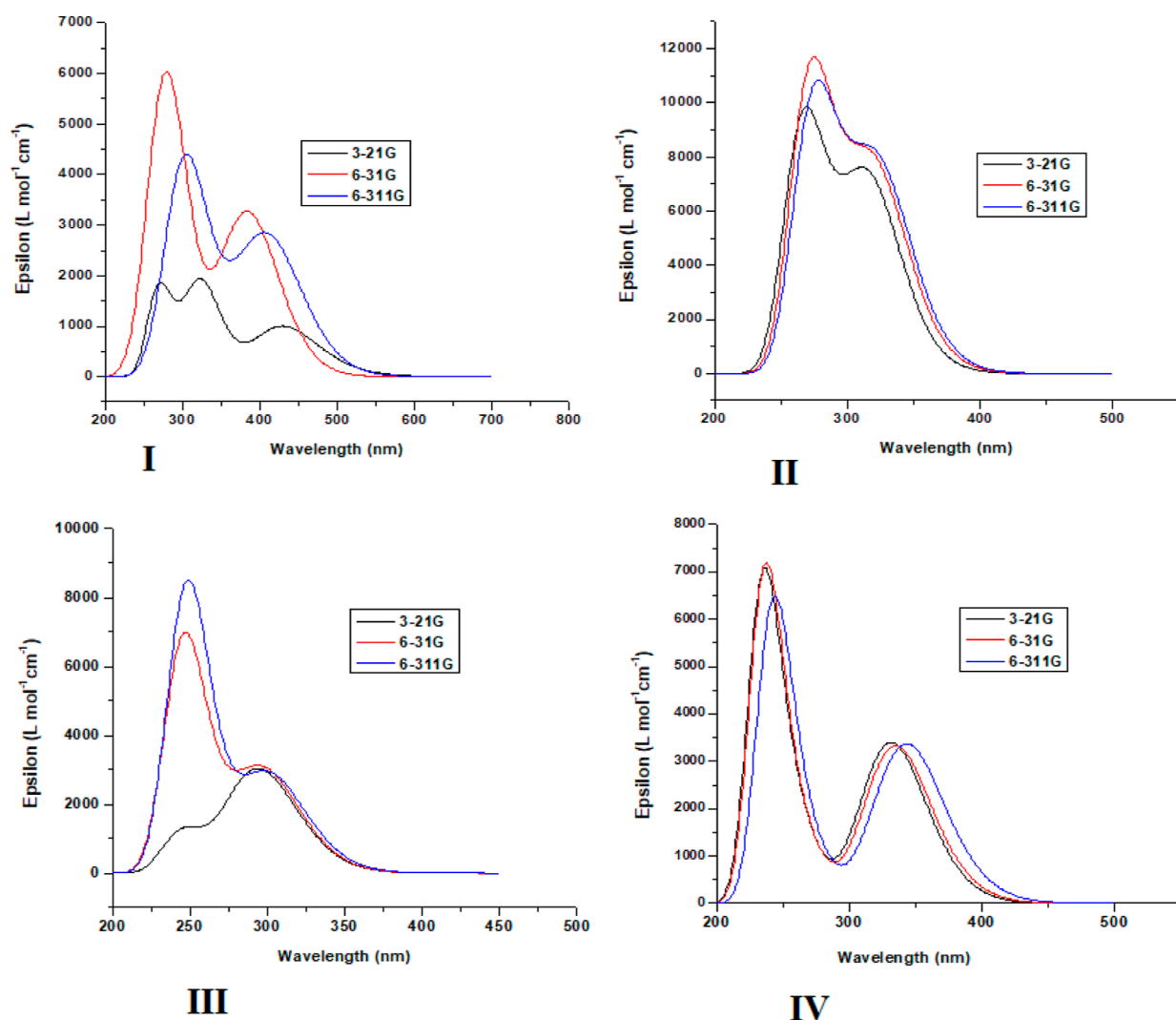
Figure 4. Comparison of UV−vis absorption spectra of polyphenols (**I−IV**) computed at different basis sets.

3.4. NBO Analysis. The natural bonding orbital analysis has been conducted with DFT/B3LYP with the 6-311G basis set and applying the "Second Order Perturbation Theory Analysis of Fock Matrix in NBO Basis" set to optimize the conjugated interactions and molecular stability. The stabilization energy values associated with delocalization between donor (i) and acceptor (j) follows the equation

$$E(2) = \Delta E_{ij} = q_i(F_i, j)/(\varepsilon_i - \varepsilon_j)2$$

$F(i,j)$ is the Fock matrix element, ε_{ii} and ε_j are the donor and acceptor diagonal elements, and q_i is orbital occupancy.[50] In NBO analysis, the highest stabilization energy value was indicated by compound (**III**) as E_2 = 43.06 kcal/mol, followed by donor O8(i) lone pair and C10−O11(j) π^* antibonding molecular orbital interaction. For compound (**II**), the stabilization energy was E_2 = 41.37 kcal/mol due to O11(i) lone pair-C9−O10(j) π^* antibonding molecular orbital interaction. Compound (**IV**) has shown a molecular stabilization energy value of E_2 = 26.89 kcal/mol associated with electron transfer from O8(i) lp to C3−C4(j) π^* antibonding molecular orbital, and for compound (**I**), it was $E2$ = 26.45 kcal/mol, followed by interaction between O7(i) Lp and C5−C6 π^* molecular orbitals contributing to the significant stability of the molecule (Table S3: Supporting

Information). The higher energy values make the molecule more stable.

3.5. UV−Vis Analysis. To design and develop the UV absorber compounds, through an insight into electronic transition of compounds, a comparative TD-DFT has been applied for polyphenolic compounds under investigation. Different basis sets have been applied, i.e., 3-21G, 6-31G, and 6-311G, for all compounds, and UV−vis absorption spectra have plotted between molar absorption coefficient (epsilon ε = L mol^{-1}·cm^{-1}) vs wavelength (λ = nm). All compounds show different peaks at different wavelengths representing electronic transitions.[51] The absorption spectra taken at different basis sets have provided in Figure 4, indicating a good coherence among only for compounds **II** and **IV**, whereas for compounds **I** and **III**, there was no coherence and a difference is observed.[36,52−54] The UV−vis absorption spectrum of natural polyphenols (**I−IV**) has been obtained by TD-DFT calculations at the ground state. By this analysis, we have established the structure−activity relationship via the delocalized π-orbital and electronic transition energy values. The maximum absorption wavelengths with corresponding oscillation strength corresponds to electronic transition from HOMO (highly occupied molecular orbitals) to LUMO (lowest unoccupied molecular orbitals). According to the
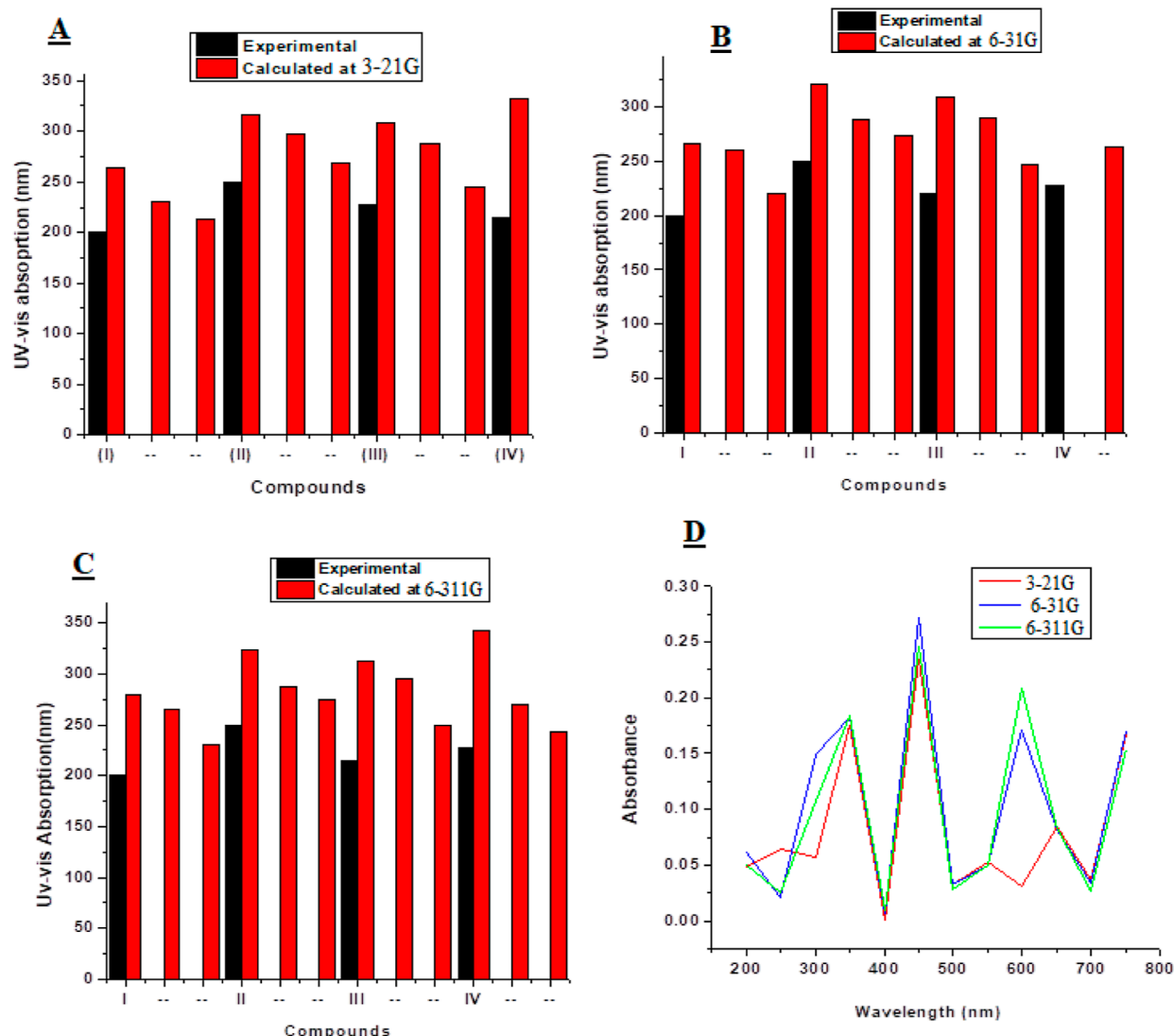
6-31G>3-21G>6-311G

Figure 5. (A−D) Wavelength vs oscillation strength plotted at different basis sets for all compounds.

FMO of compounds depicted in Figure 3, the delocalization of HOMO is mainly over π-conjugated carbon atoms of the benzene ring, while LUMO is delocalized mainly over C−O or C-substituent.[55]

The λ_{max}, oscillation strength (f), excitation energies (E), electronic transition contribution (ETC %), and relative deviation between experimental and calculated values have been provided in a tabulated form for all compounds. The computed values of λ_{max} for almost all transitions correspond to lie in $\pi−\pi^*$ (HOMO → LUMO), lower lying singlet electronic transition range.[52] In the present study, all polyphenols have shown three excited states with variable number of transitions, while the electronic transition contribution (ETC %) values have been calculated for only the largest transition coefficient (given in the output file of TD-DFT), indicating the major contribution of electronic transition for each excitation state. For the calculation of relative deviation and electronic transition contribution, the following formulas (11 and 12) have been applied.

$$RD \% = (\text{theoretical/experimental}) \times 100 - 100 \qquad (12)$$

$$ETC \% = 2 \times (\text{coefficient})2 \times 100\% \qquad (13)$$

The absorption data obtained by TD-DFT have been correlated with their corresponding experimental values for the validation of computational results.

3.5.1. Basis Set 3-21G. For basis set 3-21G, the best λ_{max} = 235.61 nm (89%) with a more intense peak responsible for HOMO → LUMO transition has been shown by compound (**IV**) in its third excitation state with the smallest relative deviation (only 3.3%) from experimental value. Similarly, compound (**II**) also depicted good absorption spectra values with smaller deviations of 26.5, 19.1, and 7.1%. Compound (**III**) has presented average values of UV−vis absorption with 44, 33.7, and 14.2% deviation, while compound (**I**) has also shown acceptable values of RD %, i.e., 32, 14.6 in the first and second transition states, respectively, indicating that good coherence with experimental data but comparatively more better absorption values has been observed for third excitation state of compound (**I**) with RD = 6%. Comparison between experimental and theoretical values at basis set 3-21G given in Table S5 (Supporting Information) has been elaborated by a

line bar provided in Figure 5A. The UV−vis absorption reliability order of compounds with respect to their experimental data at 3-21G has been shown as

IV > I > II > III

3.5.2. Basis Set 6-31G. The reliability order of computational study on the basis of RD % has been investigated with another basis set 6-31G for polyphenolic compounds; the best absorption (λ_{max} = 236.85 nm) (67.10% electronic transition) with an intense peak has been given by compound (**IV**), indicating lowest deviation from experimental data for second and third excitation states, i.e., 15.6 and 3.38%, respectively. Compound (**I**) also depicted good absorption results with RD % of 33, 29.5, and 9.92% giving peaks responsible for electronic transitions. Compounds (**II**) and (**III**) have also shown better absorption results with RD % of 28.45, 15.16, 9.92, 31.36, and 12.2, respectively, giving peaks (Figure 4) caused by $\pi-\pi^*$ transitions, while some excited states failed to produce reliable results with a greater percentage of deviation. According to the computational results of UV−vis absorption given in Table S5 (Supporting Information), the reliability or coherence order of computational and experimental data of compounds at 6-31G will be

IV > I > II > III

The relative deviation of compounds from experimental values at 6-31G has also been depicted in Figure 5B.

3.5.3. Basis Set 6-311G. Basis set 6-311G represents the best absorption at λ_{max} = 243 nm (65% $\pi-\pi^*$) with less RD = 6.6% for compound (**IV**) demonstrated in the third excitation state. Compound (**I**) showed 39.5, 32.47, and 15% RD values with fair coherence to experimental data. In the case of compound (**II**), the relative deviation showed 29.2, 14.86, and 10.22%, indicating good λ_{max}, While the first excited state of compounds (**III**) and (**IV**) failed to indicate reliable results due to higher deviation (45 and 50%) from experimental results. The computed data of UV−vis absorption have been provided in Table S5 (Supporting Information). Line bar has also been plotted to explain the relative deviation percentage of the respective compound (Figure 5C).

IV > II > I > III

The electronic transition states with degenerate orbital and smaller energy gaps between HOMO and LUMO gave more superimposed results.[56] The results of the present analysis revealed that for UV−vis computational analysis of compounds, basis sets "6-31G" and 3-21G showed more reliable results, closely correlated with experimental values and less RD % as compared to the 6-311G basis set applied (Figure 5D).[57] Thus, the reliability order for UV−vis computational analysis for different basis sets would be as

6-31G > **3-**21G > **6-**311G

4. CONCLUSIONS

Four polyphenols, i.e., catechol (**I**), caffeic acid (**II**), gallic acid (**III**), and pyrogallol (**IV**), have been extracted from *F. indica* through column chromatography and identified by GC−MS. After identification, these compounds have been subjected to computational analysis mainly by employing DFT with the 6-311G basis set and functional B3LYP. Findings through this mechanistic approach indicate higher biological reactivity of caffeic acid (**II**) with larger values of chemical softness (σ = 13.421), electronegativity (χ (eV) = −648.644), dipole moment (μ (Debye) = 4.541), electrostatic potential value (-8.424×10^{-2} to $+8.424 \times 10^{-2}$), smaller values of chemical potential (−0.269), E_{LUMO} (−0.080), and energy gap (ΔE = 0.149). The molecular geometry of compounds has also been optimized, which indicates a successful coherence to their respective experimental values of all geometric parameters. The excited-state energies and complexation sites in compounds through absorption characteristics have been investigated by application of TD-DFT and taking UV−vis spectra with 3-21G, 6-31G, and 6-311G sets. For compound (**I**), the best absorption at λ_{max} = 235.61 nm (89%) was obtained at 3-21G, compound (**IV**) indicates the best absorption for both 6-31G and 6-311G basis sets at λ_{max} = 236.85 nm (67.10% electronic transition), and λ_{max} = 243 nm (65% $\pi-\pi^*$) with less RD = 6.6%, respectively. Compounds (**II**) and (**III**) gave average results for all the three basis sets. When computational results of different basis sets were compared, the 6-31G set gave more reliable results compared to corresponding experimental values. When the structural description of polyphenols (**I−IV**) was investigated by taking their FT-IR vibrational simulations at 3-21G, 6-31G, and 6-311G, the calculated vibrational frequencies and spectra were compared with corresponding experimental values. An acceptable correlation has been observed between experimental and computed findings, thereby confirming the molecular structure of compounds. Any kind of shortcoming could be due to the different conditions in theoretical and experimental calculations. This study exhibits remarkable reactivity criterion corresponding to the chemical structure and geometry, quantum mechanical, electronic population, as well as in absorptional and vibrational spectroscopic point of view, which could facilitate further computational and experimental analyses of these essential natural compounds in the novel drug discovery field.

■ ASSOCIATED CONTENT

ⓢ Supporting Information

The Supporting Information is available free of charge at https://pubs.org/doi/10.1021/acsomega.3c06544.

Experimental and calculated vibrational frequencies of **I−IV** with different solvents; bond lengths (A^0) and bond angles (^{0}) of compounds (**I−IV**) calculated at DFT-B3LYP/6-311G compared with experimental values; second-order perturbation theory analysis of Fock matrix in NBO basis for polyphenolic compounds (**I−IV**); Mulliken charges of compounds (**I−IV**); and λ_{max} (nm), oscillation strength (f), excitation energy (E eV), relative deviation (RD %), and electronic transition contribution values for polyphenols (**I−IV**) computed for 3-21G, 6-31G, and 6-311G basis sets with the B3LYP functional (PDF)

■ AUTHOR INFORMATION

Corresponding Author

Nusrat Shafiq − *Department of Chemistry, Government College Women University, Faisalabad 38000, Pakistan;* ⊙ orcid.org/0000-0002-3270-4227; Email: dr.nusratshafiq@gcwuf.edu.pk, gqumarin@gmail.com

Authors

Rabia Riaz − *Department of Chemistry, Government College Women University, Faisalabad 38000, Pakistan*

Shagufta Parveen − *Department of Chemistry, Government College Women University, Faisalabad 38000, Pakistan*

Maryam Rashid − *Department of Chemistry, Government College Women University, Faisalabad 38000, Pakistan*

Complete contact information is available at:
https://pubs.acs.org/10.1021/acsomega.3c06544

Author Contributions

Rabia Riaz contributed to extraction, fractionation, drafting, and evaluation of results and DFT study for spectroscopic analysis; **Shagufta Parveen**[1] contributed to data analysis, literature, and proofreadings; Maryam **Rashid**[1] contributed to library data analysis, proofreading, and English check; and **Nusrat Shafiq**[1]* contributed to conceptualization, supervision, funding, corrections, proofreadings, overall final editing, and setting.

Notes

The authors declare no competing financial interest.

■ REFERENCES

(1) Iftikhar, F.; Khan, M. B. N.; Tehreem, S.; Kanwal, N.; Musharraf, S. G. BCL11A-targeted γ-globin gene induction by triterpenoid glycosides of Fagonia indica: A preclinical scientific validation of indigenous herb for the treatment of β-hemoglobinopathies. *Bioorg. Chem.* **2023**, *140*, 106768.

(2) Eman, A. A.; Gehan, H. A.; Yassin, M.; Mohamed, S. Chemical composition and antibacterial activity studies on callus of Fagonia arabica L. *Acad. Arena* **2010**, *2* (12), 91−106.

(3) Fang, Z.; Bhandari, B. Encapsulation of polyphenols-a review. *Trends Food Sci. Technol.* **2010**, *21* (10), 510−523.

(4) Qi, X.; Liu, H.; Ren, Y.; Zhu, Y.; Wang, Q.; Zhang, Y.; Wu, Y.; Yuan, L.; Yan, H.; Liu, M. Effects of combined binding of chlorogenic acid/caffeic acid and gallic acid to trypsin on their synergistic antioxidant activity, enzyme activity and stability. *Food Chem.: X* **2023**, *18*, 100664.

(5) Bhootham, V.; Gul, M. Z.; Chernapalli, V.; Rupula, K. Polyphenol Profile in different Maize varieties and their Antioxidant Potentials: Implications in Disease Resistance. *Biol. Forum—Int. J.* **2023**, *15* (5a), 441−449.

(6) Huang, W.-Y.; Cai, Y.-Z.; Zhang, Y. Natural phenolic compounds from medicinal herbs and dietary plants: potential use for cancer prevention. *Nutr. Cancer* **2009**, *62* (1), 1−20.

(7) Giglio, R. V.; Patti, A. M.; Cicero, A. F.; Lippi, G.; Rizzo, M.; Toth, P. P.; Banach, M. Polyphenols: potential use in the prevention and treatment of cardiovascular diseases. *Curr. Pharm. Des.* **2018**, *24* (2), 239−258.

(8) Li, S.; Yin, S.; Ding, H.; Shao, Y.; Zhou, S.; Pu, W.; Han, L.; Wang, T.; Yu, H. Polyphenols as potential metabolism mechanisms regulators in liver protection and liver cancer prevention. *Cell Proliferation* **2023**, *56* (1), No. e13346.

(9) Wu, M.; Luo, Q.; Nie, R.; Yang, X.; Tang, Z.; Chen, H. Potential implications of polyphenols on aging considering oxidative stress, inflammation, autophagy, and gut microbiota. *Crit. Rev. Food Sci. Nutr.* **2021**, *61* (13), 2175−2193.

(10) (a) Cornard, J.-P.; Merlin, J.-C. Molecular structure and spectroscopic properties of 4-nitrocatechol at different pH: UV-visible, Raman, DFT and TD-DFT calculations. *Chem. Phys.* **2005**, *309* (2−3), 239−249. (b) Marc, G.; Stana, A.; Tertiş, M.; Cristea, C.;

Cioriţă, A.; Drăgan, Ş.-M.; Toma, V.-A.; Borlan, R.; Focşan, M.; Pîrnău, A. Discovery of New Hydrazone-Thiazole Polyphenolic Antioxidants through Computer-Aided Design and In Vitro Experimental Validation. *Int. J. Mol. Sci.* **2023**, *24* (17), 13277.

(11) (a) Iqbal, J.; Zahra, S. T.; Ahmad, M.; Shah, A. N.; Hassan, W. Herbicidal Potential of Dryland Plants on Growth and Tuber Sproutingin Purple Nutsedge (Cyperus rotundus). *Planta Daninha* **2018**, *36*, No. e018170606. (b) Kanwal, N.; Adhikari, A.; Hameed, A.; Hafizur, R. M.; Musharraf, S. G. Isolation and characterization of non-sulfated and sulfated triterpenoid saponins from Fagonia indica. *Phytochemistry* **2017**, *143*, 151−159.

(12) (a) Ansari, A. A.; Kenne, L.; Atta-ur-Rahman. Isolation and characterization of two saponins from Fagonia indica. *Phytochemistry* **1987**, *26* (5), 1487−1490. (b) Ansari, A. A.; Kenne, L.; Atta-ur-Rahman; Wehler, T. Isolation and characterization of a saponin from Fagonia indica. *Phytochemistry* **1988**, *27* (12), 3979−3982. (c) Farheen, R.; Mahmood, I.; Siddiqui, B. S. Fagonilin: a new triterpene from fagonia indica burm. F. Var. Indica. *FUUAST J. Biol.* **2014**, *4* (2), 261.

(13) Kohn, W.; Becke, A. D.; Parr, R. G. Density functional theory of electronic structure. *J. Phys. Chem.* **1996**, *100* (31), 12974−12980.

(14) (a) Arthur, D. E.; Uzairu, A.; Mamza, P.; Abechi, S. E.; Shallangwa, G. J. B.-S. U.; Sciences, A. Insilco study on the toxicity of anti-cancer compounds tested against MOLT-4 and p388 cell lines using GA-MLR technique. *J. Basic Appl. Sci.* **2016**, *5* (4), 320−333. (b) Farag, A. M.; Fahim, A. M. Synthesis, biological evaluation and DFT calculation of novel pyrazole and pyrimidine derivatives. *J. Mol. Struct.* **2019**, *1179*, 304−314.

(15) Horchani, M.; Hajlaoui, A.; Harrath, A. H.; Mansour, L.; Ben Jannet, H.; Romdhane, A. J. New pyrazolo-triazolo-pyrimidine derivatives as antibacterial agents: Design and synthesis, molecular docking and DFT studies. *J. Mol. Struct.* **2020**, *1199*, 127007.

(16) Karunaratne, E.; Hill, D. W.; Dührkop, K.; Böcker, S.; Grant, D. F. Combining Experimental with Computational Infrared and Mass Spectra for High-Throughput Nontargeted Chemical Structure Identification. *Anal. Chem.* **2023**, *95* (32), 11901−11907.

(17) Prasetyo, W. E.; Purnomo, H.; Sadrini, M.; Wibowo, F. R.; Firdaus, M.; Kusumaningsih, T. Identification of potential bioactive natural compounds from Indonesian medicinal plants against 3-chymotrypsin-like protease (3CLpro) of SARS-CoV-2: molecular docking, ADME/T, molecular dynamic simulations, and DFT analysis. *J. Biomol. Struct. Dyn.* **2023**, *41* (10), 4467−4484.

(18) Yadav, S.; Sewariya, S.; Chandra, R.; Singh, P.; Kumar, A.; Jain, P.; Sachdeva, S.; Kumari, K. An investigation to understand the correlation between the experimental and density functional theory calculations of noscapine. *J. Phys. Org. Chem.* **2023**, *36* (7), No. e4502.

(19) Bakheit, A. H.; Abuelizz, H. A.; Al-Salahi, R. A DFT Study and Hirshfeld Surface Analysis of the Molecular Structures, Radical Scavenging Abilities and ADMET Properties of 2-Methylthio (methylsulfonyl)-[1, 2, 4] triazolo [1, 5-a] quinazolines: Guidance for Antioxidant Drug Design. *Crystals* **2023**, *13* (7), 1086.

(20) Muthu, S.; Prabhakaran, A. Vibrational spectroscopic study and NBO analysis on tranexamic acid using DFT method. *Spectrochim. Acta, Part A* **2014**, *129*, 184−192.

(21) O Ozdemir, U.; İlbiz, F.; Balaban Gunduzalp, A.; Ozbek, N.; Karagoz Genç, Z.; Hamurcu, F.; Tekin, S. J. Alkyl sulfonic acid hydrazides: Synthesis, characterization, computational studies and anticancer, antibacterial, anticarbonic anhydrase II (hCA II) activities. *J. Mol. Struct.* **2015**, *1100*, 464−474.

(22) Patuhai, A.; Wahab, P. E. M.; Yusoff, M. M.; Dewir, Y. H.; Alsughayyir, A.; Hakiman, M. Plant Growth Regulator-and Elicitor-Mediated Enhancement of Biomass and Andrographolide Production of Shoot Tip-Culture-Derived Plantlets of Andrographis paniculata (Burm. f.) Wall.(Hempedu Bumi). *Plants* **2023**, *12* (16), 2953.

(23) Atiq-ur-Rehman. GC-MS analysis of n-hexane extract of Fagonia indica Burm. f. with hypoglycaemic potential. *Nat. Prod. Res.* **2022**, *37*, 3702−3710.

(24) Frisch, M. J.; Trucks, G. W.; Schlegel, H. B.; Scuseria, G. E.; Robb, M. A.; Cheeseman, J. R.; Scalmani, G.; Barone, V.; Petersson, G. A.; Nakatsuji, H.; etal. *Gaussian 09*, Revision A.02, 2016.

(25) Manzhos, S.; Wang, X.; Carrington, T. A multimode-like scheme for selecting the centers of Gaussian basis functions when computing vibrational spectra. *Chem. Phys.* **2018**, *509*, 139−144.

(26) Rijal, R.; Sah, M.; Lamichhane, H. P. Molecular simulation, vibrational spectroscopy and global reactivity descriptors of pseudoephedrine molecule in different phases and states. *Heliyon* **2023**, *9* (3), No. e14801.

(27) Singh, J. S. IR and Raman spectra with Gaussian-09 molecular analysis of some other parameters and vibrational spectra of 5-fluorouracil. *Res. Chem. Intermed.* **2020**, *46*, 2457−2479.

(28) Wu, Q.; Yu, P.; Li, J.; Wang, Y.; Chen, K. Mechanistic elucidation of the degradation and transformation of hydroxy-α-sanshool and its conformers as the pungent dietary components in Sichuan pepper: A DFT study. *Food Chem.* **2024**, *430*, 137078.

(29) PerkinElmer. *ChemBioDraw Ultra Version*; CambridgeSoft Waltham: MA, USA, 2012.

(30) Pandey, A. K.; Dwivedi, A.; Mishra, A. K.; Tiwari, S. N.; Vuai, S. A.; Singh, V. Quantum chemical study of effect on adsorption properties of antituberculosis drug N-Cyclopentylidenepyridine-4-carbohydrazide interaction with CNT (C56H16). *J. Indian Chem. Soc.* **2023**, *100* (1), 100851.

(31) Manjusha, P.; Prasana, J. C.; Muthu, S.; Rizwana, B. F. Spectroscopic elucidation (FT-IR, FT-Raman and UV-visible) with NBO, NLO, ELF, LOL, drug likeness and molecular docking analysis on 1-(2-ethylsulfonylethyl)-2-methyl-5-nitro-imidazole: An antiprotozoal agent. *Comput. Biol. Chem.* **2020**, *88*, 107330−107360.

(32) El-Demerdash, S. H.; Halim, S. A.; El-Nahas, A. M.; El-Meligy, A. B. A density functional theory study of the molecular structure, reactivity, and spectroscopic properties of 2-(2-mercaptophenyl)-1-azaazulene tautomers and rotamers. *Sci. Rep.* **2023**, *13* (1), 15626−15717.

(33) Konappa, N.; Udayashankar, A. C.; Krishnamurthy, S.; Pradeep, C. K.; Chowdappa, S.; Jogaiah, S. GC-MS analysis of phytoconstituents from Amomum nilgiricum and molecular docking interactions of bioactive serverogenin acetate with target proteins. *Sci. Rep.* **2020**, *10* (1), 16438−16523.

(34) Ali, N.; Mansha, A.; Asim, S.; Zahoor, A. F.; Ghafoor, S.; Akbar, M. U. A computational perspective of vibrational and electronic analysis of potential photosensitizer 2-chlorothioxanthone. *J. Mol. Struct.* **2018**, *1156*, 571−582.

(35) Marrassini, C.; Idrissi, A.; De Waele, I.; Smail, K.; Tchouar, N.; Moreau, M.; Mezzetti, A. Organic solvent-luteolin interactions studied by FT-Raman, Vis-Raman, UV-Raman spectroscopy and DFT calculations. *J. Mol. Liq.* **2015**, *205*, 2−8.

(36) Selvaraj, S.; Rajkumar, P.; Thirunavukkarasu, K.; Gunasekaran, S.; Kumaresan, S. Vibrational (FT-IR and FT-Raman), electronic (UV-vis) and quantum chemical investigations on pyrogallol: A study on benzenetriol dimers. *Vib. Spectrosc.* **2018**, *95*, 16−22.

(37) Karabacak, M.; Sinha, L.; Prasad, O.; Cinar, Z.; Cinar, M. The spectroscopic (FT-Raman, FT-IR, UV and NMR), molecular electrostatic potential, polarizability and hyperpolarizability, NBO and HOMO-LUMO analysis of monomeric and dimeric structures of 4-chloro-3, 5-dinitrobenzoic acid. *Spectrochim. Acta, Part A* **2012**, *93*, 33−46.

(38) Sas, E.; Kurt, M.; Karabacak, M.; Poiyamozhi, A.; Sundaraganesan, N. FT-IR, FT-Raman, dispersive Raman, NMR spectroscopic studies and NBO analysis of 2-Bromo-1H-Benzimidazol by density functional method. *J. Mol. Struct.* **2015**, *1081*, 506−518.

(39) Socrates, G. *Infrared and Raman characteristic group frequencies: tables and charts*; John Wiley & Sons, 2004.

(40) Tosovic, J. Spectroscopic features of caffeic acid: theoretical study. *Kragujevac J. Sci.* **2017**, No. 39, 99−108.

(41) Avcı, D.; Alturk, S.; Tamer, O.; Kuşbazoğlu, M.; Atalay, Y. Solvent effect in implicit/explicit model on FT-IR, 1H, 13C and 19F NMR, UV-vis and fluorescence spectra, linear, second-and third-nonlinear optical parameters of 2-(trifluoromethyl) benzoic acid:

Experimental and computational study. *J. Mol. Struct.* **2017**, *1143*, 116−126.

(42) Muthu, S.; Prabhakaran, A. Vibrational spectroscopic study and NBO analysis on tranexamic acid using DFT method. *Spectrochim. Acta, Part A* **2014**, *129* (14), 184−192.

(43) Sayin, K.; Üngördü, A.; Spectroscopy, B. Investigation of anticancer properties of caffeinated complexes via computational chemistry methods. *Spectrochim. Acta, Part A* **2018**, *193*, 147−155.

(44) Abbaz, T.; Bendjeddou, A.; Villemin, D. Density Functional Theory Studies On Molecular Structure And Electronic Properties Of sulfanilamide, Sulfathiazole, E7070 And Furosemide Molecules. *IOSR J. Appl. Chem.* **2019**, *12*, 60.

(45) Rizwana B, F.; Muthu, S.; Prasana, J. C.; Abraham, C. S.; Raja, M. Spectroscopic (FT-IR, FT-Raman) investigation, topology (ESP, ELF, LOL) analyses, charge transfer excitation and molecular docking (dengue, HCV) studies on ribavirin. *Chem. Data Collect.* **2018**, *17−18* (18), 236−250.

(46) Ajeel, F. N.; Khudhair, A. M.; Mohammed, A. A. Density functional theory investigation of the physical properties of dicyano pyridazine molecules. *Int. J. Sci. Res.* **2015**, *4* (1), 2334−2339.

(47) Honarparvar, B.; Pawar, S. A.; Alves, C. N.; Lameira, J.; Maguire, G. E.; Silva, J. R. A.; Govender, T.; Kruger, H. G. J. J. o. b. s. Pentacycloundecane lactam vs lactone norstatine type protease HIV inhibitors: binding energy calculations and DFT study. **2015**, *22* (1), 15, .

(48) Zeyrek, C. T.; Koçak, S. B.; Ünver, H.; Pektaş, S.; Başterzi, N. S.; Çelik, Ö. Molecular structure and density functional modelling studies of 2-[(E)-2-(4-hydroxyphenyl) ethyliminomethyl] phenol. *J. Mol. Struct.* **2015**, *1100*, 570−581.

(49) Bendjeddou, A.; Abbaz, T.; Gouasmia, A.; Villemin, D.; Chemistry, A. Molecular structure, HOMO-LUMO, MEP and Fukui function analysis of some TTF-donor substituted molecules using DFT (B3LYP) calculations. *Int. Res. J. Pure Appl. Chem.* **2016**, *12*, 1−9.

(50) Bağlan, M.; Goren, K.; Yildiko, U. HOMO-LUMO, NBO, NLO, MEP analysis and molecular docking using DFT calculations in DFPA molecule. *Int. J. Chem. Technol.* **2023**, *7* (1), 38−47.

(51) Pathan, H. K.; Khanum, G.; Javed, R.; Siddiqui, N.; Selvakumari, S.; Muthu, S.; Ali, A.; Arora, H.; Afzal, M.; Kumar, A.; et al. Quantum Computational, Spectroscopic Characterization, Hirshfeld Analysis & Molecular docking Studies on p-Toluenesulfonic Acid (p-TSA) or Tosylic Acid. *Chem. Phys. Impact* **2023**, *7*, 100320−100412.

(52) Anouar, E. H.; Gierschner, J.; Duroux, J. L.; Trouillas, P. UV/Visible spectra of natural polyphenols: A time-dependent density functional theory study. *Food Chem.* **2012**, *131* (1), 79−89.

(53) Catauro, M.; Barrino, F.; Dal Poggetto, G.; Crescente, G.; Piccolella, S.; Pacifico, S. New SiO2/caffeic acid hybrid materials: Synthesis, spectroscopic characterization, and bioactivity. *Materials* **2020**, *13* (2), 394.

(54) Andjelkovic, M.; Van Camp, J.; De Meulenaer, B.; Depaemelaere, G.; Socaciu, C.; Verloo, M.; Verhe, R. Iron-chelation properties of phenolic acids bearing catechol and galloyl groups. *Food Chem.* **2006**, *98* (1), 23−31.

(55) Kose, E.; Atac, A.; Karabacak, M.; Nagabalasubramanian, P.; Asiri, A.; Periandy, S. FT-IR and FT-Raman, NMR and UV spectroscopic investigation and hybrid computational (HF and DFT) analysis on the molecular structure of mesitylene. *Spectrochim. Acta, Part A* **2013**, *116*, 622−634.

(56) Rangan, S.; Katalinic, S.; Thorpe, R.; Bartynski, R. A.; Rochford, J.; Galoppini, E. Energy level alignment of a Zinc (II) tetraphenylporphyrin dye adsorbed onto TiO2 (110) and ZnO (1120) surfaces. *J. Phys. Chem. C* **2010**, *114* (2), 1139−1147.

(57) Zara, Z.; Iqbal, J.; Ayub, K.; Irfan, M.; Mahmood, A.; Khera, R. A.; Eliasson, B. A comparative study of DFT calculated and experimental UV/Visible spectra for thirty carboline and carbazole based compounds. *J. Mol. Struct.* **2017**, *1149*, 282−298.